Research Article | Vol. 27, No. 20 | 30 Sep 2019 | OPTICS EXPRESS 28091
Optics EXPRESS

Polarization envelope helicity dependent photovoltage in GaAs/$Al_{0.3}Ga_{0.7}As$ modulation-doped quantum well

HIRONORI ITO,[1] TETSUO NAKANO,[2] SHINTARO NOMURA,[2,*] AND KAZUHIKO MISAWA[1]

[1]*Department of Applied Physics, Tokyo University of A&T, Koganei, Tokyo 184-8588, Japan*
[2]*Division of Physics, University of Tsukuba, Tennodai, Tsukuba, Ibaraki 305-8571, Japan*
[*]*nomura.shintaro.ge@u.tsukuba.ac.jp*

Abstract: In this study, we demonstrate the switching of the direction of the photocurrent in an *n*-type GaAs/$Al_{0.3}Ga_{0.7}As$ modulation-doped quantum well using a polarization pulse-shaping apparatus containing a $4f$ setup. The right- and left- polarization-twisting pulses with a polarization rotation frequency in the THz-regime are incident on a modulation-doped quantum well. The results show that the sign of the photovoltage is dependent on the direction of rotation of the polarization-twisting pulses, which can be explained by the circular photogalvanic effect combined with the production of a classical edge photocurrent from the acceleration of free electrons in the vicinity of the sample edge by the incident optical electric field. The wide range over which the polarization-rotation frequency may be tuned makes this method a powerful tool to investigate the response of an extensive variety of materials in the THz-regime.

© 2019 Optical Society of America under the terms of the OSA Open Access Publishing Agreement

1. Introduction

Manipulating the polarization and waveform of the electromagnetic field of optical pulses has attracted significant attention as a method of controlling electronic states and specific vibrational modes of matter. Recently developed pulse shaping methods enable us to control temporal evolution of the amplitude and direction of the electromagnetic field vectors in a prescribed manner [1–3]. Despite their potential wide applicability to investigations of molecules, dielectrics, and metals, investigations of properties of solid state materials using vector shaped pulses remain in an initial stage. Here we demonstrate that the arbitrary control of the electromagnetic field is indeed a powerful tool to control the motion of the electrons in semiconductors.

In contrast to the high controllability of electromagnetic fields, controlling the angular momentum of electrons in nonmagnetic semiconductors has witnessed limited success. In one attempt, the circularly polarized terahertz waves were used to optically control the angular momentum of electrons in semiconductors. In this approach, the circular polarization of the incident THz wave changed the direction of the photocurrent induced by the circular photogalvanic effect [4–6]. In addition, the asymmetric scattering of the carriers by an incident oscillating electric field allows the direction of the photocurrent along the sample edge to be controlled by an incident circular-polarized THz wave [7]. However, these experiments used laboratory THz sources with limited frequency ranges. For example, the frequency range of a transversely excited atmospheric-pressure-CO_2 laser is typically from 27 to 33 THz [5], and an optically pumped molecular gas laser using NH_3, CH_3F, and D_2O has discrete lines from 1 to 25 THz [8]. In THz wave generation by optical rectification, the tunability of the THz radiation is only limited by the phase-matching condition imposed by noncollinear interactions inside a nonlinear crystal [9] and the bandwidth of the fs laser spectrum.

Polarization pulse shaping uses a $4f$ set-up and spatial light modulators (SLMs) to independently control the phases of each frequency component of an electromagnetic field [1, 2], thereby

#369541 https://doi.org/10.1364/OE.27.028091
Journal © 2019 Received 7 Jun 2019; revised 9 Aug 2019; accepted 29 Aug 2019; published 19 Sep 2019

Optics EXPRESS

controlling the polarization and frequency of an optical pulse. One notable example of a polarization-shaped pulse is a polarization-twisting pulse (PTP), where the major axis of polarization rotates at a fixed angular frequency. PTPs, with their wide continuously tunable polarization-rotation frequency from 0 to 50 THz, may open up the possibility of using optical pulses to control electron motion in semiconductors. To free ourselves from the phase-matching condition, we use the impulsive stimulated Raman scattering induced by PTPs to directly excite electrons in a GaAs crystal. In this way, the phase-matching condition is relaxed because the long interaction length in the crystal that is necessary to emit THz radiation is not required for impulsive stimulated Raman scattering.

The helicity of the envelope of a PTP has been shown to transfer an angular momentum of $\pm 2\hbar$ to the material through impulsive stimulated Raman scattering [10]. In another study, the pseudorotational motion of the lattice was directly observed by using PTPs to excite the Raman-active rotational modes of α-quartz [11], and a prescribed terahertz polarization waveform was generated by the optical rectification of PTPs propagating along the three-fold axis of a [111] GaP crystal [3]. Irradiation by a right-envelope-helicity PTP induces an angular momentum $\Delta J_z = -2\hbar$ by impulsive stimulated Raman scattering, and the rotational analog of the Umklapp process of the three-fold axis adds $\Delta J_z = 3\hbar$; therefore, $\Delta J_z = \hbar$ is induced in the material [10,12].

An example of the Raman scattering response of conduction electrons to THz radiation without involving the circular-polarization selection rule, is the strong signal from single-particle intersubband transitions of the electrons in a quantum well, which has been observed in the spectra of resonant Raman scattering [13] and which is explained theoretically in Ref. [14]. Specifically, conduction subbands are spin-split in the momentum direction by the spin-orbit interaction. However, intersubband transitions via Raman scattering with the circular-polarization selection rule enforced (i.e., transfer of angular momentum) has not been clarified or demonstrated. Angular-momentum transfer via impulsive stimulated Raman scattering is not possible with linearly polarized light or circularly polarized light but is only possible with PTPs [12]. Furthermore, photoelastic modulators have been used to phase modulate near-infrared pulses; this technique can now be extended to modulating the helicity of PTPs. Such a system can then be used to modulate the angular momentum of the recipient matter via stimulated Raman scattering and has the advantage of focusing on spin-selective phenomena with intersubband transitions in the THz range. Conversely, the circular photogalvanic effect occupies a vital role in the investigation of the spin states of intersubband transitions. [4,5] The spin selection rule is reflected in the direction of the current created by the conduction-band electrons.

In this paper, we present an experimental study of the photovoltage induced by irradiating an n-type modulation-doped quantum well (MDQW) with PTPs. The results show that the direction of the photocurrent generated in an n-type MDQW by PTP irradiation switches direction in accordance with the direction of the helicity of the polarization envelope. We demonstrate that polarization pulse shaping constitutes a powerful method to investigate the response of a wide variety of materials in the THz-regime.

2. Experimental and background of the method

The sample consisted of a 400×1600 μm^2 Hall-bar structure of (001) GaAs/$Al_{0.3}Ga_{0.7}As$ n-type MDQW with 10 nm well width. Eighteen ohmic contacts were prepared as shown schematically in Fig. 1(a). The photovoltage was probed by using two of the contacts, and the unused contacts remained open. The electron density and the mobility of the sample were 2.6×10^{15} m^{-2} and 310 000 cm^2 V^{-1}s^{-1}, respectively, as estimated by a Hall measurement at 0.3 K with zero backgate voltage ($V_g = 0.0$ V).

Optical pulses from a mode-locked fs Ti:sapphire laser were fed into a $4f$ setup for the arbitrary vector field shaping [3]. The spectral range of the optical pulses was from 700 to 900 nm. The phases of $\theta_{\pm 45^\circ}(\omega)$ of the diagonally polarized components of each frequency ω were controlled

Optics EXPRESS

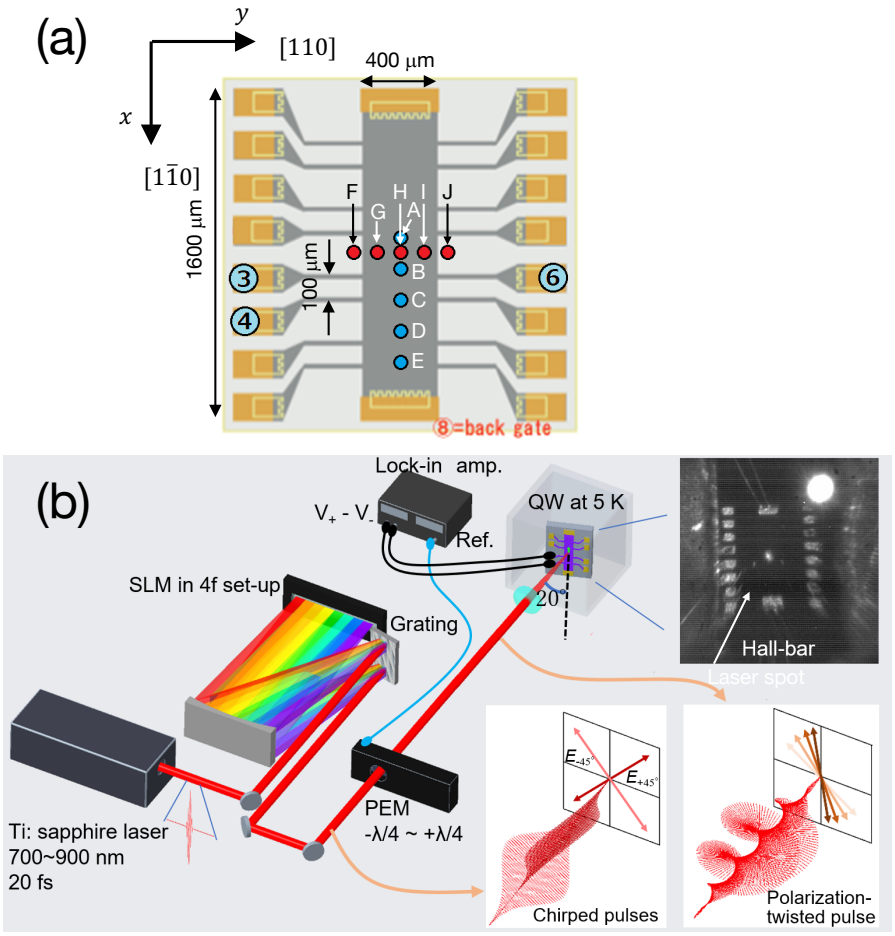

Fig. 1. (a) Schematic diagram of the sample Hall-bar structure. The voltage probe pairs 3-4 and 3-6 were used to measure the photovoltage. The blue solid circles A to E are the positions of the center of the illumination spot aligned at the center of the stem of the Hall-bar. The red solid circles F to J are the positions of the center of the illumination spot aligned parallel to the y direction. (b) Schematic drawing of experimental setup. 20-fs pulses are introduced into the $4f$ setup to disperse the frequency components. The spectral phase $\theta_{\pm 45^\circ}(\omega)$ is set by the SLM to generate PTPs. The envelope helicity of the pulses is modulated by the PEM to obtain a retardation between $-\lambda/4$ and $+\lambda/4$. The pulses are incident on the Hall-bar sample in a He cryostat at 5 K at an oblique angle of 20°. The position of the Hall-bar sample is moved with a three-axis mechanical stage at a fixed laser beam position. The photovoltage is detected by a lock-in amplifier synchronized with the PEM. The small white point at the center of the Hall-bar in the optical micrograph captured by the monochrome CCD camera is the excitation laser spot. The electric field vector of the PTP is also shown.

independently by using dual-pixel masks of SLMs as

$$E_{\pm 45^\circ}(t)\hat{\mathbf{e}}_{\pm 45^\circ} = \int \frac{d\omega}{2\pi} e^{-i\omega t}\tilde{E}_{\mathrm{inc}}(\omega)e^{i\theta_{\pm 45^\circ}(\omega)}\hat{\mathbf{e}}_{\pm 45^\circ} \tag{1}$$

where $\hat{\mathbf{e}}_{\pm 45^\circ} = \frac{1}{\sqrt{2}}[\hat{\mathbf{e}}_x \pm \hat{\mathbf{e}}_y]$ is the direction of the axis of the pixel masks of the SLM, $\hat{\mathbf{e}}_x$ and $\hat{\mathbf{e}}_y$ are unit vectors with directions along the positive x- and y-axis, respectively, and $\tilde{E}_{\mathrm{inc}}(\omega)$ is the

Optics EXPRESS

Fourier-transform-limited incident pulse, as schematically shown in Fig. 2(a).

After passing through a quarter-wave plate, the output electric field is

$$\begin{pmatrix} E_x(t) \\ E_y(t) \end{pmatrix} = \int \frac{d\omega}{2\pi} e^{-i\omega t} \tilde{E}_{\text{inc}}(\omega) e^{i\theta_{\text{opt}}(\omega)} \begin{pmatrix} \cos\phi_{\text{opt}}(\omega) \\ \sin\phi_{\text{opt}}(\omega) \end{pmatrix} \tag{2}$$

where $\theta_{\text{opt}}(\omega) = \frac{1}{2}(\theta_{45^\circ}(\omega) + \theta_{-45^\circ}(\omega))$ is spectral phase, $\phi_{\text{opt}}(\omega) = \frac{1}{2}(\theta_{45^\circ}(\omega) - \theta_{-45^\circ}(\omega))$ is the angle of linear polarization with respect to the vertical direction. To generate PTPs, we introduce an optical pulse with the following spectral parameters into the SLM:

$$\theta_{\text{opt}}(\omega) = \frac{\beta}{2}(\omega - \omega_0)^2, \tag{3}$$

$$\phi_{\text{opt}}(\omega) = \gamma(\omega - \omega_0) \tag{4}$$

where ω_0 is the laser center frequency. The spectral phase in Eq. (3) describes a linear chirp that stretches the optical pulse width in the time domain as $\tau(\omega) = (\partial/\partial\omega)\theta_{\text{opt}}(\omega) = \beta(\omega - \omega_0)$. In the experiment, the group delay dispersion was $-16\,000$ fs^2, and the pulse duration was 3.0 ps. The instantaneous frequency $\omega_{\text{ins}}(t)$ is well defined in the time domain in this case as the inverse function of $t = \tau(\omega)$. The modulation in Eq. (4) rotates the instantaneous linear-polarization angle $\phi_{\text{opt}}(\omega_{\text{ins}}(t)) = \gamma\beta^{-1}t$ as shown in Fig. 2(b).

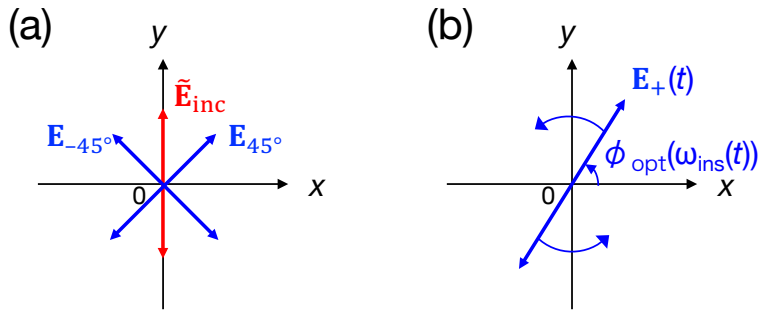

Fig. 2. (a) Directions of the linearly polarized incident electric field ($\tilde{\mathbf{E}}_{\text{inc}}$) and the diagonally polarized electric fields ($\mathbf{E}_{\pm 45^\circ}(t)$). Dual-pixel masks of SLMs control the phases $\theta_{\pm 45^\circ}(\omega)$ of the diagonally polarized components of each frequency ω. (b) Polarization direction of the left-envelope-helicity PTP ($\mathbf{E}_+(t)$) rotating as $\phi_{\text{opt}}(\omega_{\text{ins}}(t)) = \gamma\beta^{-1}t$.

Impulsive stimulated Raman scattering may be treated classically [15] for an electron with displacement $\mathbf{q}(t)$. The nonlinear susceptibility χ_e may be expanded as

$$\chi_e = \chi_{e0} + (\nabla\chi_e)\cdot\mathbf{q}(t) + (\nabla^2\chi_e)\mathbf{q}(t)\cdot\mathbf{q}(t) + \cdots . \tag{5}$$

We assume small $\mathbf{q}(t)$ and leave only the first two terms, then the energy stored in the electron polarization is given by

$$U(t) = -\frac{1}{2}\epsilon_0[\chi_{e0} + \nabla\chi_e\cdot\mathbf{q}(t)]\mathbf{E}(t)\cdot\mathbf{E}(t). \tag{6}$$

The force acting on the electron is

$$\mathbf{F}(t) = -\nabla U(t) = \frac{\epsilon_0}{2}\nabla\chi_e(\mathbf{E}(t)\cdot\mathbf{E}(t)) \tag{7}$$

Optics EXPRESS

where we assume that the incident electric field $\mathbf{E}(t)$ has two component angular frequencies ω_1 and ω_2 as $\mathbf{E}(t) = \mathbf{E}_1(t)e^{-i\omega_1 t} + \mathbf{E}_2(t)e^{-i\omega_2 t}$ with slowly varying envelope functions $\mathbf{E}_1(t)$ and $\mathbf{E}_2(t)$.

In the quantum mechanical description, the selection rules for impulsive stimulated Raman scattering induced by a laser pulse are based on conservation of the spin angular momentum of the photons [12]. For $\omega > 0$, $E_j(\omega)$ and $E_j^*(\omega)$ correspond to annihilation and creation of photons with polarization state j, respectively, where $j = +(-)$ denotes left-circular (right-circular) polarization, as defined by $E_\pm(\omega) \equiv \frac{1}{\sqrt{2}}[\tilde{E}_x(\omega) \mp i\tilde{E}_y(\omega)]$. For example, a PTP with Stokes frequency Ω and left envelope helicity annihilates left-circularly polarized photons with frequency ω and creates of a right-circularly polarized photon with frequency $\omega - \Omega$ as described by $E_-^*(\omega - \Omega)E_+(\omega)$. Using the relation of $E_\pm(\omega) = E_\mp^*(-\omega)$, we obtain

$$E_-^*(\omega - \Omega)E_+(\omega) = E_+(\Omega - \omega)E_+(\omega). \tag{8}$$

In this case, the angular momentum of the matter irradiated by the PTP must change by $\pm 2\hbar$. When the rotational axis is three-fold, the crystal provides an angular momentum of $\pm 3\hbar$, as demanded by its rotational symmetry. Therefore, the rotation of vector fields with angular momentum of $+\hbar$ $(-\hbar)$ can be selectively excited by using $-2\hbar$ $(+2\hbar)$ [10]. The Stokes frequency of the Raman scattered photon from the incident PTP is twice the rotational frequency of the instantaneous linear polarization, and is varied from 0 to 50 THz in these experiments.

The helicity of the PTP was modulated at 50 kHz by using a photoelastic modulator (PEM). We carefully aligned the optics to avoid any intensity modulation on the optical pulses at the sample surface. In addition, we made an independent verification that the modulation of the pulse intensity after passing through the PEM was less than 10^{-5} of the incident intensity of the pulses. The helicity dependent photovoltage was detected synchronously by using a lock-in amplifier with the phase determined by using a reference photodiode. The shaped pulses impinged on the surface of a Hall-bar structure consisting of a (001) GaAs/$Al_{0.3}Ga_{0.7}$As MDQW held at 5 K in a He cryostat. The sample was excited at oblique incidence at the angle of $\Theta_0 = 20^\circ$ with respect to the $[\bar{1}\bar{1}0]$ direction, as shown schematically in Fig. 1(b). The position of the Hall-bar sample was moved with a three-axis mechanical stage at a fixed laser beam position. The position of the laser spot on the sample surface was monitored by using a monochrome CCD camera, as shown in inset A of Fig. 1(b). The laser spot appears as a small white spot at the center of the Hall-bar structure. The laser spot on the surface of the sample was measured about 100 μm in diameter.

3. Results and discussion

3.1. Photovoltage induced by below-band-gap polarization twisted pulses

The photocurrent induced in a MDQW structure by circularly polarized electromagnetic irradiation is described by [4]

$$\vec{J} = \overleftrightarrow{\gamma} \cdot \hat{e}E^2 P_{\text{circ}}, \tag{9}$$

where $\overleftrightarrow{\gamma}$, $\hat{e}$, E, and P_{circ} are the pseudo-tensor, direction of propagation of the laser beam, amplitude of the optical electric field, and degree of circular polarization, respectively. Given the symmetry of a (001) quantum well optically illuminated by a laser beam propagating in the (y, z) plane, the photocurrent in the x direction is

$$j_x = \gamma_{xy} t_p t_s \sin\Theta_0 E^2 P_{\text{circ}}/n, \tag{10}$$

where Θ_0 is the angle of incidence, n is the index of refraction of the GaAs/$Al_{0.3}Ga_{0.7}$As sample, and t_p, and t_s are the Fresnel transmission coefficients for linear p and s polarization, respectively. As described previously, irradiation by a PTP creates an electromagnetic field at frequency Ω, which induces a photocurrent in the excitation spot, as described by Eq. (6). In other words, the

Optics EXPRESS

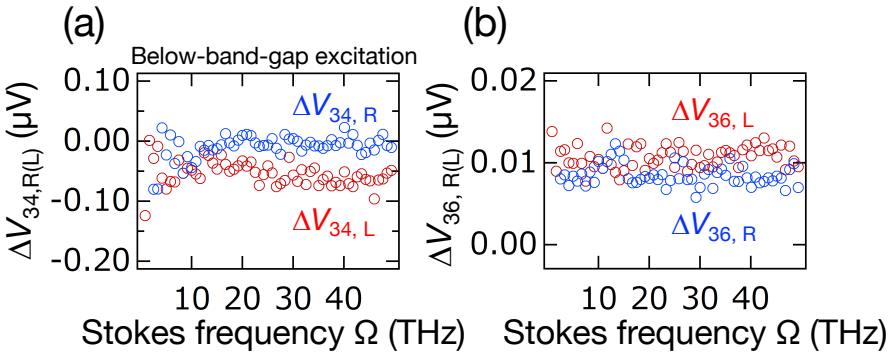

Fig. 3. (a) Photovoltage signal $\Delta V_{34,R(L)}$ measured between contacts 3 and 4, and (b) $\Delta V_{36,R(L)}$ measured between contacts 3 and 6 as functions of the Stokes frequency of the PTPs for below-band-gap excitation between 825 and 900 nm at pulse energy of 131 pJ. Data points plotted are $\Delta V_{34,R} = V_{34,R} - V_{34,L}$ at $\gamma > 0$ and $\beta > 0$ (blue circles), and $\Delta V_{34,L} = V_{34,L} - V_{34,R}$ at $\gamma < 0$ and $\beta > 0$ (red circles) in (a), and $\Delta V_{36,R} = V_{36,R} - V_{36,L}$ (blue circles), and $\Delta V_{36,L} = V_{36,L} - V_{36,R}$ (red circles) in (b).

excitation spot is equivalent to a current generator, and this current induces a voltage between the voltage probes, which is measured by the lock-in amplifier.

Figure 3 shows the results for a photovoltage $V_{34} \equiv V_3 - V_4$ induced by irradiation by PTPs propagating in the y-z plane at the an off-resonance frequency below the band gap of the GaAs QW (i.e., between 825 and 900 nm) at pulse energy of 131 pJ. This figure corresponds to the laser excitation spot B in Fig. 1(a). Here, V_i is the voltage at contact i in Fig. 1, and $V_{34,R}$ ($V_{34,L}$) is the photovoltage V_{34} induced by right-envelope-helicity (left-envelope-helicity) PTPs impinging between contacts 3 and 4. The change $\Delta V_{34,R} = V_{34,R} - V_{34,L}$ in photovoltage was detected as a function of the envelope Stokes frequency for each direction of the envelope helicity of the incident PTP. After reversing the helicity of PTPs by changing the settings for the SLM, thus changing the sign of γ in Eq. (4), $\Delta V_{34,L} = V_{34,L} - V_{34,R}$ was detected. The results show that $\Delta V_{34,L}$ is less than $\Delta V_{34,R}$ for a PTP Stokes frequency greater than 15 THz as shown in Fig. 3(a). In contrast, $\Delta V_{36,L}$ is greater than $\Delta V_{36,R}$ for most of the data points in Fig. 3(b). These results suggest that the change in photovoltage depends on the helicity of the angular momentum transferred to the conduction electrons through impulsive stimulated Raman scattering [10, 15]. However, the direction of the photovoltage is obscured by the constant floor of the difference in voltages of about $-0.03\mu V$ and 0.01 μV in Figs. 3(a) and 3(b), respectively, which is possibly due to noise accumulation in the measurements.

3.2. *Photovoltage induced by on-resonant polarization twisted pulses*

It is widely accepted that a factor of 10^3-10^4 times enhancement of the Raman scattering peak at single-particle intersubband transition can be observed by resonantly exciting the direct gap of semiconductors [13]. The enhancement factor was explained by considering the full resonance situation including both the valence and conduction bands [14]. We therefore conducted resonant Raman scattering measurements to enhance the photovoltage signal by irradiation with PTPs. Figure 4 shows the photovoltage signals $\Delta V_{34,R}$ and $\Delta V_{34,L}$ between contacts 3 and 4 induced by irradiation by PTPs propagating in the y-z plane for resonant excitation between 700 and 900 nm at pulse energy of 27 pJ. We checked that the photovoltage signals $\Delta V_{34,R}$ and $\Delta V_{34,L}$ are proportional to the square of the laser excitation power, as expected for the impulsive stimulated Raman scattering. First, we focus on the case that gives the largest signal. Figure 4(b) corresponds to excitation spot B in Fig. 1. A factor of 600 times enhancement of the photovoltage signals is

Optics EXPRESS

observed due to the on-resonant excitation as estimated from $|\Delta V_{34,R} - \Delta V_{34,L}|$ in Figs. 3(a) and 4(b) at 49.3 THz. By correcting the factor of the pulse energy $(131\text{pJ}/27\text{pJ})^2$, the enhancement of the photovoltage signals by on-resonant excitation is 14 000, which is in reasonable agreement with the theory [14].

We note that electron-hole pairs generated by on-resonant excitation and photogenerated carriers may contribute to the dc photovoltage $V_{34,R}$ and $V_{34,L}$. This dc photovoltage of the orders of mV is larger than the photovoltage signals in Fig. 4. The difference between $V_{34,R}$ and $V_{34,L}$ has been detected by using the PEM, which modulates the retardation of the laser pulses alternatively between $\lambda/4$ and $-\lambda/4$ at a frequency of 50 kHz. With this technique, the envelope helicity-dependent signals $\Delta V_{34,R}$ and $\Delta V_{34,L}$ are detected at a high sensitivity by excluding the signal due to the one-photon excitation, which is envelope helicity-independent. The valence hole plays a large role in enhancing the resonant Raman scattering, however, the contribution of the optically generated valence-holes for the observed right- and left-envelope-helicity dependence of the photovoltage is small because the angular momentum of photon is not transferred to the valence hole by the one-photon excitation with the PTPs.

We confirmed that the sign of the change in photovoltage reverses upon changing the sign of γ in Eq. (4) by changing the setting of the SLM to reverse the envelope helicity of the PTP. [see plot in Fig. 4(b); red circles]. This result clearly demonstrates that the direction of the photocurrent in the Hall-bar sample is controlled by the envelope helicity of the PTPs. Note that the change in photovoltage occurs only for irradiation at oblique incidence but is absent at normal incidence.

The sign of the photovoltage is consistent with the circular photogalvanic effect when a sample is irradiated by circular THz pulses with photon energy less than the separation between subbands in the conduction band [4, 5]. The circular photogalvanic effect is caused by the k-term linear in k in the electron Hamiltonian, which is due to the Dresselhaus [16] and/or Rashba [17–19] spin-orbit interactions and which gives splittings in k_x, as shown in Fig. 5. The transition from e_1 to e_2 is forbidden for excitation at normal incidence in an n-type (001)-grown GaAs quantum well with $\sigma^+(\sigma^-)$ polarization. At oblique incidence the intraband transition from e_1 to e_2 is allowed; however, the simple selection rules do not hold because of the lower symmetry. At oblique incidence, the rates of these transitions differ at k_+ and k_- [5], as illustrated by different thickness of the arrows in Fig. 5. The asymmetric distribution of carriers in k space induces a photocurrent j_x in the x direction. The helicity of circularly polarized THz pulses corresponds to angular momentum ΔJ_z transferred to the matter. The direction of the photocurrent generated by σ^- ($\Delta J_z = +\hbar$) irradiation at $\theta_0 = 20^\circ$ is in the $[1\bar{1}0]$ direction [4] when the excitation energy is less than the separation between the e_1 and e_2 subbands. We carefully confirmed the helicity of the PTPs and the direction of photocurrent. The helicity is defined from the point of view of the receiver. The polarization of right-envelope-helicity PTPs rotates counterclockwise when observed from the light source as shown schematically in Fig. 6(a). Figure 4(b) indicates that $\Delta V_{34,R} > 0$, so the current j_x flows from contact 3 to 4 in the external circuit when the Hall-bar is illuminated by right-envelope-helicity PTPs. Assuming that the angular momentum $\Delta J_z = -2\hbar$ due to stimulated Raman scattering by right-envelope-helicity PTPs is added with the angular momentum $\Delta J_z = 3\hbar$ due to the Umklapp process of the three-fold axis, the total angular momentum is $\Delta J_z = \hbar$. In this case, the irradiation with $\Delta J_z = \hbar$ at $\Theta_0 = 20^\circ$ generates a photocurrent in the $[1\bar{1}0]$ direction, which is consistent with the circular photogalvanic effect.

The photovoltage signal in Fig. 4(b) that depends on the envelope helicity of the PTPs is induced by the stimulated Raman scattering caused by the single-particle intersubband transitions of the electrons in the quantum well. The Stokes frequency Ω is related to the intersuband energy separation of the conduction electron between the subbands e_1 and e_2 in Fig. 5. The photovoltage signal is expected to increase close to $\Omega \approx E_{21}$, where E_{21} is the energy spacing between e_1 and e_2, and decrease at the higher Ω side. Figure 4(b) shows that the change $\Delta V_{34,R} = V_{34,R} - V_{34,L}$ in the photovoltage increases monotonically up to around 50 THz (blue

Optics EXPRESS

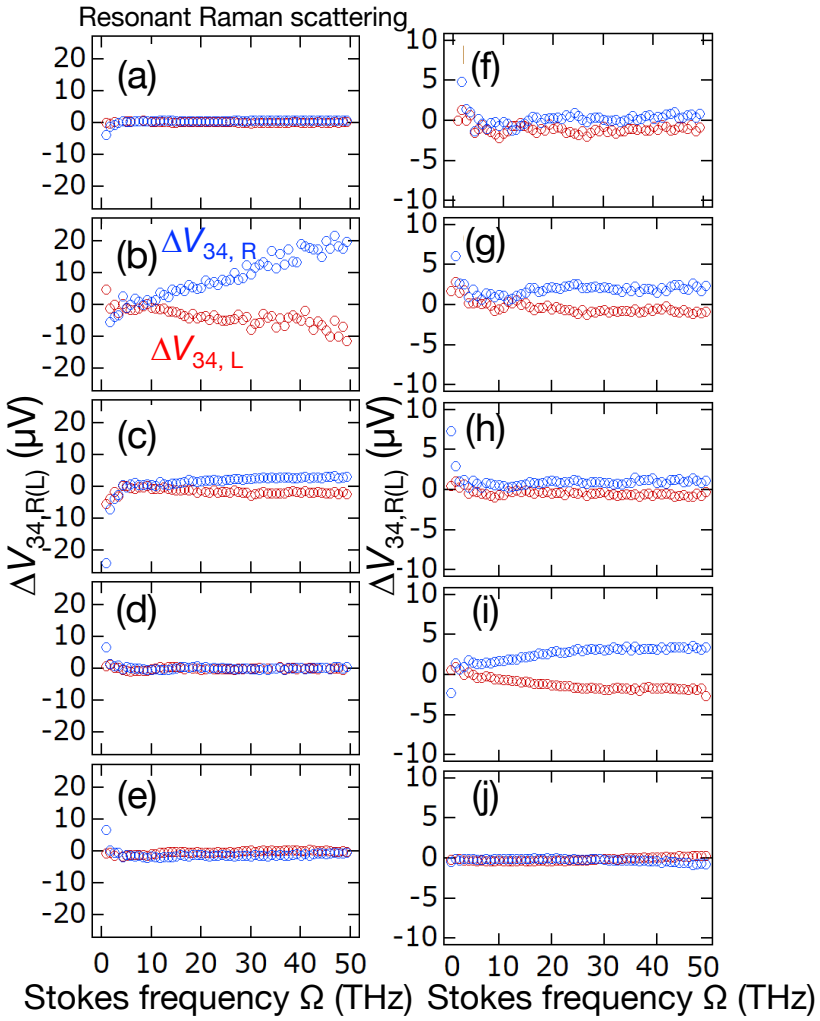

Fig. 4. Photovoltage signal $\Delta V_{34,R(L)}$ measured between contacts 3 and 4 as functions of the Stokes frequency of PTPs for resonant excitation between 700 and 900 nm at pulse energy of 27 pJ for the laser excitation spot A-J as schematically shown in Fig. 1(a). Data points are plotted for $\Delta V_{34,R} = V_{34,R} - V_{34,L}$ at $\gamma > 0$ and $\beta > 0$ (blue circles), and $\Delta V_{34,L} = V_{34,L} - V_{34,R}$ at $\gamma < 0$ and $\beta > 0$ (red circles).

circles). The Stokes frequency Ω dependence of the photovoltage signal in Fig. 4 reflects the inhomogeneous distribution of the width of the quantum well structure and the instantaneous spectral width of the PTPs.

3.3. Dependence of photovoltage on beam spot position

In order to further understand the underlining mechanisms of the observed photovoltage, we have conducted measurements of photovoltage at various beam spot position on the Hall-bar sample. Figures 4(a)–4(e) show the photovoltage signal for the beam-spot positions A–E in Fig. 1(a), respectively. The spacing between each spot was 150 μm. Laser beam-spot position dependence at point A–E of photovoltage signal $\Delta V_{34,R}$ and $\Delta V_{34,L}$ at Ω = 49.3 THz is shown in Fig. 8(a). The photovoltage signal is largest for the beam spot at position B in Fig. 1(a), which is close to

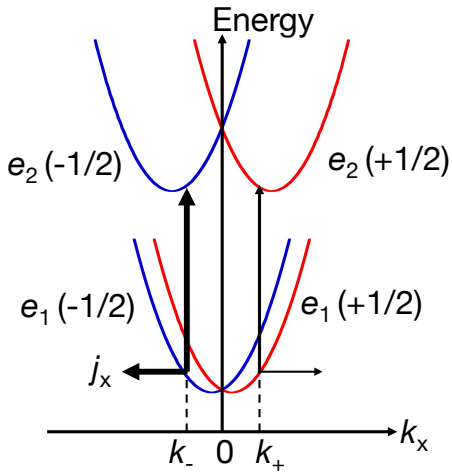

Fig. 5. Schematics of conduction-band electron subband structures with k-term linear in k and the transitions between the subbands e_1 and e_2 with spins $\pm 1/2$ induced by the σ^+ excitations.

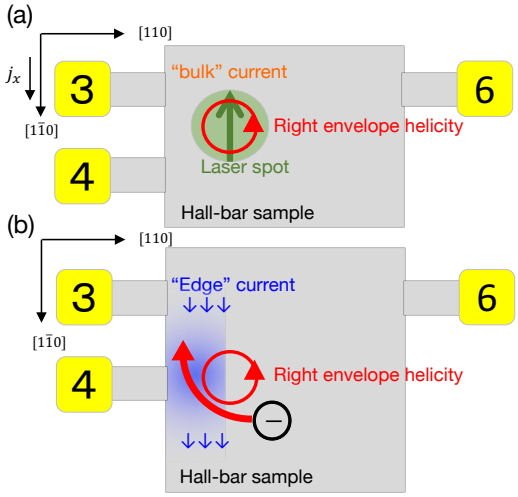

Fig. 6. Schematic illustrations of (a) photocurrent induced by the circular photogalvanic effect and (b) classical edge photocurrent generated by the acceleration of free carriers in the vicinity of the sample edge by the optical electric field.

the line connecting contacts 3 and 6. A similar dependence on the excitation frequency, but with a smaller signal occurs with the beam spot at point C, which is slightly below contact 4 [see Fig. 1(a)]. No signal was detected when the beam spot was at points A, D, or E.

Figures 4(f)–4(j) show $\Delta V_{34,R(L)}$ between contacts 3 and 4 for beam spots F–J from Fig. 1(a), respectively. Laser beam-spot position dependence at point F–J of photovoltage signal $\Delta V_{34,R}$ and $\Delta V_{34,L}$ at $\Omega = 49.3$ THz is also shown in Fig. 8(b). The spacing between each spot was 120 μm. Figures 4(f)–4(j) show that $\Delta V_{34,R(L)}$ was greatest when the right half side of the Hall-bar

structure at spot I was illuminated. Smaller signals were detected with the beam spot at points G and H.

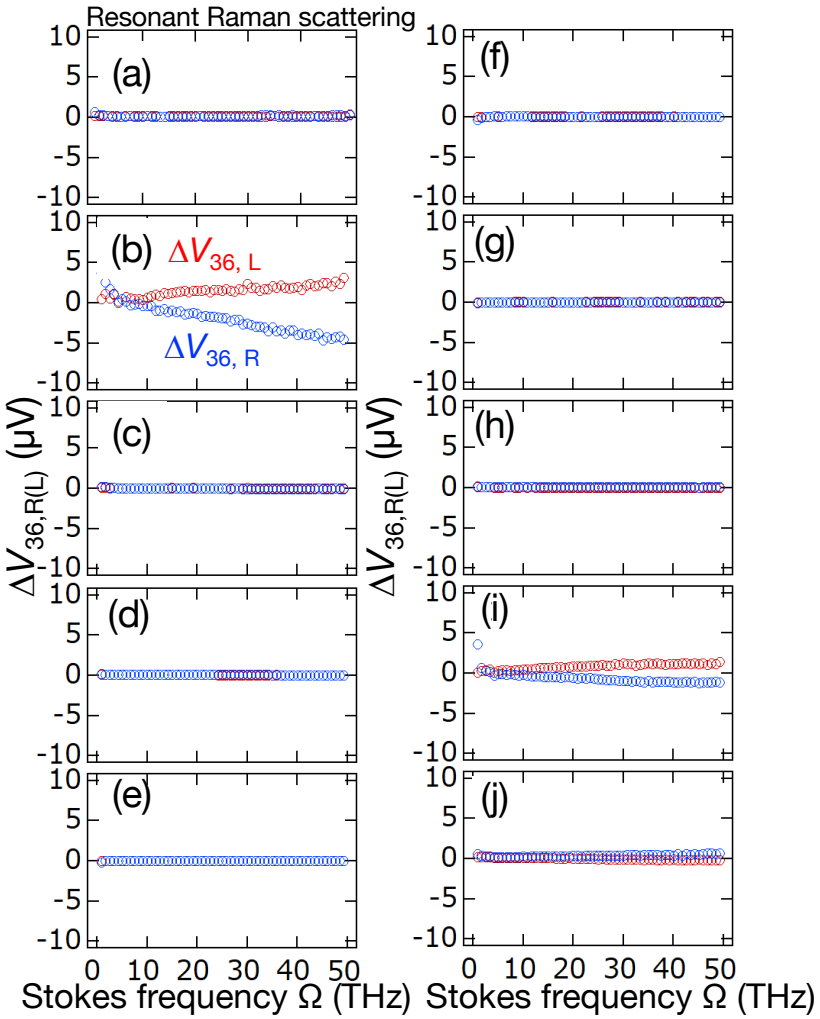

Fig. 7. Photovoltage signal $\Delta V_{36,R(L)}$ measured between contacts 3 and 6 as functions of the Stokes frequency of PTPs for resonant excitation between 700 and 900 nm for the laser excitation spot positioned at point A–J on the Hall-bar structure [see Fig. 1(a)]. Data points are plotted for $\Delta V_{36,R} = V_{36,R} - V_{36,L}$ at $\gamma > 0$ and $\beta > 0$ (blue circles), and $\Delta V_{36,L} = V_{36,L} - V_{36,R}$ at $\gamma < 0$ and $\beta > 0$ (red circles).

The photovoltage signal $V_{36} \equiv V_3 - V_6$ was measured between contacts 3 and 6, and $\Delta V_{36,R} = V_{36,R} - V_{36,L}$ and $\Delta V_{36,L} = V_{36,L} - V_{36,R}$ are shown in Figs. 7(a)–7(j) for various beam-spot positions. Laser beam-spot position dependence at point A–J of photovoltage signal $\Delta V_{36,R}$ and $\Delta V_{36,L}$ at $\Omega = 49.3$ THz is summarized in Fig. 8. As for Fig. 4, the photovoltage signal is greatest when the beam spot is at position B of Fig. 1, whereas no signal is detected with the beam spot at positions A, C–E of Fig. 1. In addition, the maximal photovoltage for the beam spot positions F–J occurs with the beam spot at position I.

The dependence of photovoltage on beam spot position in Figs. 4, 7, and 8 is not fully explained solely by the circular photogalvanic effect. Another possible scenario to explain this effect is that

Optics EXPRESS

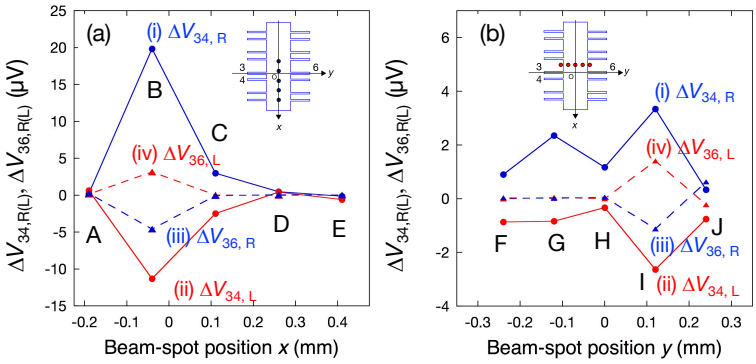

Fig. 8. (a) Laser beam-spot position dependence at point A–E of photovoltage signal (i) $\Delta V_{34,R}$ (blue circles), (ii) $\Delta V_{34,L}$ (red circles), (iii) $\Delta V_{36,R}$ (blue triangles), and (iv) $\Delta V_{36,L}$ (red triangles) at $\Omega = 49.3$ THz. (b) Laser beam-spot position dependence at point F–J of photovoltage signal (i) $\Delta V_{34,R}$ (blue circles), (ii) $\Delta V_{34,L}$ (red circles), (iii) $\Delta V_{36,R}$ (blue triangles), and (iv) $\Delta V_{36,L}$ (red triangles) at $\Omega = 49.3$ THz. The insets indicate schematic diagram of the laser beam-spot positions on the sample Hall-bar structure. The origin of the coordinate system is set at the crossing of the center of the Hall-bar and the line connecting contacts 3 and 6.

the classical edge photocurrent is added to the current from the circular photogalvanic effect. The classical edge photocurrent was observed previously in graphene [7] and is attributed to the acceleration of free carriers in the vicinity of the sample edge by the THz electric field $\mathbf{E}_{\mathrm{THz}}(t)$, similar to the surface photogalvanic effect observed on the surface of bulk GaAs [20]. This classical edge photocurrent is described by a theory based on Boltzmann's kinetic equation using the distribution function $f(\mathbf{p}, x, t)$ as,

$$\frac{\partial f}{\partial t} + v_x \frac{\partial f}{\partial x} + q\mathbf{E}_{\mathrm{THz}}(t)\frac{\partial f}{\partial \mathbf{p}} = Q\{f\}, \tag{11}$$

where $\mathbf{p}$, x, q, and v_x are the momentum, coordinate, charge, and the velocity of the carrier, respectively, and $Q\{f\}$ is the collision integral [7, 20].

Based on this theory, the first order in $\mathbf{E}_{\mathrm{THz}}(t)$ correction does not contribute to a dc current. The observed photocurrent is determined by the second order $\mathbf{E}_{\mathrm{THz}}(t)$-field correction to $f(\mathbf{p}, x, t)$ [7]. Instead of the direct acceleration of free carriers by $\mathbf{E}_{\mathrm{THz}}(t)$, the force $\mathbf{F}(t)$ in Eq. (7) acts on the electrons through the impulsive stimulated Raman process in the classical treatment upon the irradiation of the PTPs. The observed photocurrent is determined by the second order in $\mathbf{F}(t)$, proportional to the square of the laser excitation power. According to this scenario, electrons near the left edge of the sample are accelerated in the $-x$ direction, so they contribute to a positive j_x photocurrent after excitation by right-envelope-helicity PTPs as shown schematically in Fig. 6(b). This photocurrent partly cancels the photocurrent by the circular photogalvanic effect. The electrons near the right edge are accelerated in the $+x$ direction, so a photocurrent is induced in the $-x$ direction, which is the same direction as the photocurrent induced by the circular photogalvanic effect. The net result is a large signal observed when the beam spot is at position I in Fig. 4(i). The results shown in Figs. 7(b) and 7(i) indicate that the photovoltage $V_6 > V_3$ is induced by right-envelope-helicity PTPs. Constructive (destructive) photovoltage at the right (left) edge near contact 6 (3) explains these observations.

Optics EXPRESS

4. Conclusion

The results reported herein demonstrate that through impulsive stimulated Raman scattering, a vector-shaped optical pulse becomes a powerful tool for controlling electrons in a MDQW. The results indicate that the direction of the photocurrent depends on the envelope helicity of the PTPs. These observations are explained by invoking the circular photogalvanic effect combined with classical edge photocurrent generated by acceleration of free carriers in the vicinity of the sample edge by the optical electric field of the PTP. The wide range over which we can tune the frequency of the rotation of the PTP in the THz-regime and the flexibility allowed for controlling the polarization make this method particularly attractive for investigating the response of a wide variety of materials in the THz-regime. Examples of interesting problems to be explored with a vector-shaped optical pulse may be the unusual electromagnetic response, in particular the anomalous Hall effect in Weyl semimetals [21–23] and the topological phases of narrow gap transition metal dichalcogenides such as TiS_2 and $TiTe_2$ [24, 25].

Funding

Grant-in-Aid for Scientific Research from the Japan Society for the Promotion of Science (JP15H02117, JP15H03673, JP18K03487).

Acknowledgments

We acknowledge the stimulating discussion in the meeting of the Cooperative Research Project of the Research Institute of Electrical Communication, Tohoku University. T. N. and S. N. would like to thank the Open Facility Network Office, Research Facility Center for Science and Technology, University of Tsukuba, for allowing us to use facilities for sample fabrication.

Disclosures

The authors declare that there are no conflicts of interest related to this article.

References

1. T. Brixner, G. Krampert, T. Pfeifer, R. Selle, G. Gerber, M. Wollenhaupt, O. Graefe, C. Horn, D. Liese, and T. Baumert, "Quantum control by ultrafast polarization shaping," Phys. Rev. Lett. **92**, 208301 (2004).
2. T. Suzuki, S. Minemoto, T. Kanai, and H. Sakai, "Optimal control of multiphoton ionization processes in aligned I_2 molecules with time-dependent polarization pulses," Phys. Rev. Lett. **92**, 133005 (2004).
3. M. Sato, T. Higuchi, N. Kanda, K. Konishi, K. Yoshioka, T. Suzuki, K. Misawa, and M. Kuwata-Gonokami, "Terahertz polarization pulse shaping with arbitrary field control," Nat. Photon. **7**, 724 (2013).
4. S. D. Ganichev, E. L. Ivchenko, S. N. Danilov, J. Eroms, W. Wegscheider, D. Weiss, and W. Prettl, "Conversion of spin into directed electric current in quantum wells," Phys. Rev. Lett. **86**, 4358–4361 (2001).
5. S. D. Ganichev, V. V. Bel'kov, P. Schneider, E. L. Ivchenko, S. A. Tarasenko, W. Wegscheider, D. Weiss, D. Schuh, E. V. Beregulin, and W. Prettl, "Resonant inversion of the circular photogalvanic effect in n-doped quantum wells," Phys. Rev. B **68**, 035319 (2003).
6. H. Diehl, V. A. Shalygin, V. V. Bel'kov, C. Hoffmann, S. N. Danilov, T. Herrle, S. A. Tarasenko, D. Schuh, C. Gerl, W. Wegscheider, W. Prettl, and S. D. Ganichev, "Spin photocurrents in (110)-grown quantum well structures," New J. Phys. **9**, 349 (2007).
7. J. Karch, C. Drexler, P. Olbrich, M. Fehrenbacher, M. Hirmer, M. M. Glazov, S. A. Tarasenko, E. L. Ivchenko, B. Birkner, J. Eroms, D. Weiss, R. Yakimova, S. Lara-Avila, S. Kubatkin, M. Ostler, T. Seyller, and S. D. Ganichev, "Terahertz radiation driven chiral edge currents in graphene," Phys. Rev. Lett. **107**, 276601 (2011).
8. E. Ziemann, S. D. Ganichev, W. Prettl, I. N. Yassievich, and V. I. Perel, "Characterization of deep impurities in semiconductors by terahertz tunneling ionization," J. Appl. Phys. **87**, 3843–3849 (2000).
9. T. Tanabe, K. Suto, J. Nishizawa, K. Saito, and T. Kimura, "Tunable terahertz wave generation in the 3- to 7-THz region from gap," Appl. Phys. Lett. **83**, 237–239 (2003).
10. T. Higuchi, H. Tamaru, and M. Kuwata-Gonokami, "Selection rules for angular momentum transfer via impulsive stimulated raman scattering," Phys. Rev. A **87**, 013808 (2013).
11. K. Misawa, "Applications of polarization-shaped femtosecond laser pulses," Adv. Phys. X **1**, 544–569 (2016).
12. T. Higuchi, N. Kanda, H. Tamaru, and M. Kuwata-Gonokami, "Selection rules for light-induced magnetization of a crystal with threefold symmetry: The case of antiferromagnetic NiO," Phys. Rev. Lett. **106**, 047401 (2011).

Optics EXPRESS

13. A. Pinczuk, S. Schmitt-Rink, G. Danan, J. P. Valladares, L. N. Pfeiffer, and K. W. West, "Large exchange interactions in the electron gas of GaAs quantum wells," Phys. Rev. Lett. **63**, 1633–1636 (1989).
14. S. Das Sarma and D.-W. Wang, "Resonant raman scattering by elementary electronic excitations in semiconductor structures," Phys. Rev. Lett. **83**, 816–819 (1999).
15. A. M. Weiner, *Ultrafast Optics* (John Wiley and Sons, 2009), chap. 9, pp. 499–505, 2nd ed.
16. G. Dresselhaus, "Spin-orbit coupling effects in zinc blende structures," Phys. Rev. **100**, 580–586 (1955).
17. Y. Bychkov and E. Rashba, "Properties of a 2D electron gas with lifted spectral degeneracy," Sov. Phys. JETP. **39**, 66 (1984).
18. J. Nitta, T. Akazaki, H. Takayanagi, and T. Enoki, "Gate control of spin-orbit interaction in an inverted $In_{0.53}Ga_{0.47}As/In_{0.52}Al_{0.48}As$ heterostructure," Phys. Rev. Lett. **78**, 1335–1338 (1997).
19. T. Koga, J. Nitta, T. Akazaki, and H. Takayanagi, "Rashba spin-orbit coupling probed by the weak antilocalization analysis in InAlAs/InGaAs/InAlAs quantum wells as a function of quantum well asymmetry," Phys. Rev. Lett. **89**, 046801 (2002).
20. V. Alperovich, V. N. Belinicher, V. Novikov, and A. Terekhov, "Surface photovoltaic effect in gallium arsenide," JETP Lett. **31**, 546–549 (1980).
21. A. A. Burkov and L. Balents, "Weyl semimetal in a topological insulator multilayer," Phys. Rev. Lett. **107**, 127205 (2011).
22. M. M. Vazifeh and M. Franz, "Electromagnetic response of Weyl semimetals," Phys. Rev. Lett. **111**, 027201 (2013).
23. B. Q. Lv, H. M. Weng, B. B. Fu, X. P. Wang, H. Miao, J. Ma, P. Richard, X. C. Huang, L. X. Zhao, G. F. Chen, Z. Fang, X. Dai, T. Qian, and H. Ding, "Experimental discovery of Weyl semimetal TaAs," Phys. Rev. X **5**, 031013 (2015).
24. Z. Zhu, Y. Cheng, and U. Schwingenschlögl, "Topological phase diagrams of bulk and monolayer $TiS_{2-x}Te_x$," Phys. Rev. Lett. **110**, 077202 (2013).
25. A. Carvalho, R. M. Ribeiro, and A. H. Castro Neto, "Band nesting and the optical response of two-dimensional semiconducting transition metal dichalcogenides," Phys. Rev. B **88**, 115205 (2013).

133.51.140.12 {ts '2020-03-10 01:08:55'}